# Imaging of broadband terahertz beams using an array of antenna-coupled microbolometers operating at room temperature

**Jonathan Oden,[1] Jérome Meilhan,[2] Jérémy Lalanne-Dera,[2] Jean-François Roux,[1,*] Frédéric Garet,[1] Jean-Louis Coutaz,[1] and François Simoens[2]**

[1]*IMEP-LAHC, UMR-CNRS 5130, University of Savoie, 73376 Le Bourget du Lac Cedex, France*
[2] *CEA-Leti, Minatec Campus, 17 rue des Martyrs, 38054 Grenoble Cedex 9, France*
[*]*roux@univ-savoie.fr*

**Abstract:** We present results of 2D real-time imaging of terahertz (THz) beam generated by a photoconductive antenna driven by a femtosecond oscillator. The detector, operating at room temperature, is a 320 x 240 array of antenna-coupled microbolometers with integrated CMOS read-out electronics delivering 25 images per second. High quality images of broadband THz beams covering the 0.1-2 THz range are recorded while maintaining a signal-to-noise ratio of 10 for detected THz power as low as 25 nW. The compactness of the easy-to-use uncooled camera makes it very useful for the alignment of systems such as THz time-domain spectrometers and for the characterization of emitters, optics and other components.



**OCIS codes:** (040.2235) Far infrared or terahertz; (040.6808) Thermal (uncooled) IR detectors, arrays and imaging; (110.6795) Terahertz imaging.

## References and Links

1. B. B. Hu, M. C. Nuss, and B. B. Hu, "Imaging with terahertz waves," Opt. Lett. **20**(16), 1716–1718 (1995).
2. P. U. Jepsen, D. G. Cooke, and M. Koch, "Terahertz spectroscopy and imaging - modern techniques and applications," Laser & Photon. Rev. **5**(1), 124–166 (2011).
3. A. W. M. Lee, B. S. Williams, Q. Hu, and J. L. Reno, "Real-time imaging using a 4.3-THz quantum cascade laser and a 320 X 240 microbolometer focal-plane array," IEEE Photon. Technol. Lett. **18**(13), 1415–1417 (2006).
4. E. Grossman, C. Dietlein, J. Ala-Laurinaho, M. Leivo, L. Gronberg, M. Gronholm, P. Lappalainen, A. Rautiainen, A. Tamminen, and A. Luukanen, "Passive terahertz camera for standoff security screening," Appl. Opt. **49**(19), E106–E120 (2010).
5. T. May, G. Zieger, S. Anders, V. Zakosarenko, H.-G. Meyer, M. Schubert, M. Starkloff, M. Rößler, G. Thorwirth, and U. Krause, "Safe VISITOR: VISible, Infrared and Terahertz Object Recognition for security screening application," Proc. SPIE **7309**, 73090E, 73090E-8 (2009).
6. F. Rodriguez-Morales, S. Yngvesson, R. Zannoni, E. Gerecht, D. Gu, N. Wadefalk, and J. Nicholson, "Development of Integrated HEB/MMIC Receivers for Near-Range Terahertz Imaging," IEEE Trans. Microw. Theory Tech. **54**(6), 2301–2311 (2006).
7. See http://www.ophiropt.com/user_files/laser/beam_profilers/Pyroelectric-array-camera.pdf
8. S. Sankaran and K. O. Kenneth, "Schottky barrier diodes for millimeter wave detection in a foundry CMOS process," IEEE Electron Device Lett. **26**(7), 492–494 (2005).
9. L. Minkevičius, V. Tamošiunas, I. Kašalynas, D. Seliuta, G. Valušis, A. Lisauskas, S. Boppel, H. G. Roskos, and K. Köhler, "Terahertz heterodyne imaging with InGaAs-based bow-tie diodes," Appl. Phys. Lett. **99**(13), 131101 (2011).
10. F. Schuster, D. Coquillat, H. Videlier, M. Sakowicz, F. Teppe, L. Dussopt, B. Giffard, T. Skotnicki, and W. Knap, "Broadband terahertz imaging with highly sensitive silicon CMOS detectors," Opt. Express **19**(8), 7827–7832 (2011).
11. U. R. Pfeiffer, "Silicon CMOS/SiGe transceiver circuits for THz applications," in *Proceedings of IEEE 12th Topical Meeting on Silicon Monolithic Integrated Circuits in RF Systems* (Institute of Electrical and Electronics Engineers, New York, 2012), pp. 159–162.
12. F. Simoens, T. Durand, J. Meilhan, P. Gellie, W. Maineult, C. Sirtori, S. Barbieri, H. Beere, and D. Ritchie, "Terahertz imaging with a quantum cascade laser and amorphous-silicon microbolometer array," Proc. SPIE **7485**, 74850M, 74850M-10 (2009).
13. J. Meilhan, S. Pocas, J.-L. Ouvrier-Buffet, T. Maillou, P. Gellie, and S. Barbieri, "THz uncooled microbolometer array development for active imaging and spectroscopy applications," in *Proceedings of IEEE 35th International*

#177935 - $15.00 USD Received 11 Oct 2012; revised 19 Nov 2012; accepted 3 Dec 2012; published 20 Feb 2013

*Conference on Infrared Millimeter and Terahertz Waves* (Institute of Electrical and Electronics Engineers, New York, 2010), pp. *1–2.*
14. N. Oda, "Uncooled bolometer-type THz focal plane array and camera for real-time imaging," C. R. Phys. **11**(7-8), 496–509 (2010).
15. M. Bolduc, M. Terroux, L. Marchese, B. Tremblay, E. Savard, M. Doucet, H. Oulachgar, C. Alain, H. Jeronimek, and A. Bergeron, "THz imaging and radiometric measurements using a microbolometer-based camera," in *Proceedings of IEEE 36th International Conference on Infrared Millimeter and Terahertz Waves* (Institute of Electrical and Electronics Engineers, New York, 2011), pp. 1–2.
16. J. F. Molloy, M. Naftaly, and R. A. Dudley, "Characterization of Terahertz Beam Profile and Propagation," IEEE J. Sel. Top. Quantum Electron. (to be published).
17. L. Duvillaret, F. Garet, and J.-L. Coutaz, "A reliable method for extraction of material parameters in terahertz time-domain spectroscopy," IEEE J. Sel. Top. Quantum Electron. **2**(3), 739–746 (1996).
18. F. Simoens, J. Meilhan, B. Delplanque, S. Gidon, G. Lasfargues, J. Lalanne Dera, D. T. Nguyen, J.-L. Ouvrier-Buffet, S. Pocas, T. Maillou, O. Cathabard, and S. Barbieri, "Real-time imaging with THz fully-customized uncooled amorphous-silicon microbolometer focal plane arrays," Proc. SPIE **8363**, 83630D, 83630D-12 (2012).
19. D. T. Nguyen, F. Simoens, J.-L. Ouvrier-Buffet, J. Meilhan, and J.-L. Coutaz, "Broadband THz uncooled antenna-coupled microbolometer array – electromagnetic design, simulations and measurements," IEEE Trans. THz Sci. Technol. **2**, 299–305 (2012).
20. See http://www.laserquantum.com for more information about the TeraSed photoconductive emitter.
21. A. Dreyhaupt, S. Winnerl, M. Helm, and T. Dekorsy, "Optimum excitation conditions for the generation of high-electric-field terahertz radiation from an oscillator-driven photoconductive device," Opt. Lett. **31**(10), 1546–1548 (2006).
22. J. Z. Xu and X.-C. Zhang, "Optical rectification in an area with a diameter comparable to or smaller than the center wavelength of terahertz radiation," Opt. Lett. **27**(12), 1067–1069 (2002).
23. This concept of effective area is useful when no simple mathematical description of the beam shape can be given. For instance, considering pixels which side is of unity length, a 2D Gaussian beam of diameter 2w (calculated at $e^{-1}$) with magnitude of 1 will support a total energy of $\pi w^2$, so its effective area $S_{eff}$ would also be $\pi w^2$. This obviously implies that a Gaussian beam can be approximated by a cylinder of diameter 2w, as it is often done in optics. Finally, let us note that for linear THz-matter interaction this normalized coefficient $S_{eff}$ should be independent of the excitation power.
24. B. Clough, J. Liu, and X.-C. Zhang, ""All air-plasma" terahertz spectroscopy," Opt. Lett. **36**(13), 2399–2401 (2011).
25. P. Kužel, M. A. Khazan, and J. Kroupa, "Spatiotemporal transformations of ultrashort terahertz pulses," J. Opt. Soc. Am. B **16**(10), 1795–1800 (1999).
26. Because of different excitation parameters, the emitted THz power was reduced by a factor of 2.66 for the experimental data plotted in Fig. 7(b) and 7(c), as compared to the data plotted in Fig. 7(a).
27. M. Naftaly, R. E. Miles, and P. J. Greenslade, "TeraHertz transmission in polymer materials – a data library," in *Proceedings of IEEE 32th International Conference on Infrared, Millimeter, and Terahertz Waves* (Institute of Electrical and Electronics Engineers, New York, 2007), pp. 819–820.
28. J. Meilhan, F. Simoens, J. Lalanne Dera, S. Gidon, G. Lasfargues, D. T. Nguyen, and J. L. Ouvrier-Buffet, "Terahertz frequency agility of uncooled antenna-coupled micro-bolometer arrays," in *Proceedings of IEEE 37th International Conference on Infrared, Millimeter, and Terahertz Waves* (Institute of Electrical and Electronics Engineers, New York, 2012).

## 1. Introduction

Terahertz (THz) imaging, initially developed for space applications such as radio astronomy, constitutes a promising technology for many large volume applications in various domains such as security, medicine, industrial quality control, art conservative studies, etc. In the last years, since the pioneering work by B. B. Hu and M. C. Nuss, most of the published THz images were recorded with a scanning system using a single pixel detector [1,2]. Nevertheless, this technique is nowadays more and more substituted by a direct record of the THz image with an array of sensors. Arrays ensure much faster acquisition and hence can provide THz video output [3]. Small arrays of superconducting pixels, mostly based on transition edge sensors, have been integrated on focal planes [4,5]. Such cryogenic sensors comply with the very high sensitivity required for passive THz imaging but, because of their limited number of pixels, video output implies a fast opto-mechanical scanning of the scene of interest. Moreover, they operate at a very low temperature and the commercial viability of cryogenically cooled sensors remains an open question. Room-temperature matrix sensors are more practical for realistic market applications. Several technologies are in competition. Low-noise millimeter-wave monolithic integrated circuits (MMIC) can provide very sensitive heterodyne detection but still developments have to be done to keep sensitivity at higher frequencies and to fabricate arrays at moderate cost [6]. Rather cheap pyroelectric and

#177935 - $15.00 USD Received 11 Oct 2012; revised 19 Nov 2012; accepted 3 Dec 2012; published 20 Feb 2013

thermopile detector cameras are commercialized but their sensitivity is limited to $45\,\mathrm{nW}/\sqrt{\mathrm{Hz}}$ per pixel [7]. Schottky [8] and bow-tie diodes [9] are promising in terms of performances and integration, as they are compatible with microelectronics technology, but they still require additional improvement. First cameras based on CMOS transistors are very attractive but their noise equivalent power (NEP) of the order of 10's of nW [10,11] has still to be improved. Today, arrays of microbolometers [12–15] constitute certainly the best technical choice. They exhibit a very good NEP – of the order of tens of pW–, include a large number of pixels (up to $8 \times 10^4$) and operate at video rate (20~30 fps). Moreover, as they are extrapolated from the infrared technology, they benefit from the well-mastered infrared manufacturing process and from all the read-out procedures developed for thermal imaging.

Most of the papers cited above have presented characterizations of focal plane arrays (FPA) detectors using monochromatic THz sources such as Quantum Cascade Laser (QCL) or far infrared optically-pumped lasers delivering mW-range powers. In this paper, we show that a camera integrating an array of THz optimized antenna-coupled microbolometers can be used to image the beam delivered by an optoelectronical THz time-domain spectroscopy (THz-TDS) set up. Actually, imaging of such signals is of particular interest [16], because THz-TDS spectrometers become widespread and there is still a lack of easy-to-use imaging instrument that would help the user to finely adjust these optical systems. Indeed, in THz-TDS it is of prime importance to get well collimated THz beams as the numerical extraction of material parameters is conventionally done within the plane wave approximation [17]. As compared to more conventional imaging experiment, here the signal is pulsed and its spectrum usually covers more than a decade while its average power is typically weaker than a few µW. Nevertheless, the sensitivity of our microbolometers allows us to get a video image of the THz beam and to observe its shape when focused by a quasi-optical system. These highly sensitive microbolometers have been developed at CEA-Leti with a specific design for THz detection based on an innovative use of antennas and resonant cavity, resulting in sensitivity improvement and frequency agility.

In section 2, we present the principle and the technological design of the detector. We put special emphasis on the parameters that are important for the detection of broadband, low power beams, such as spectral responsivity and power threshold detection. Section 3 is devoted to the presentation of the optoelectronic set-up used to generate and shape the THz pulses. In section 4, we demonstrate the imaging of such signals and address the case of very low power signals while the images of beam spots focused by mean of different optics are finally shown as an example of application.

## 2. Presentation of the microbolometer array

### *2.1 Principle of single pixel operation*

The THz pixel consists in the association of an uncooled high-performance bolometer microbridge architecture and of a crossed antennas structure. This structure makes the device sensitive to any impinging radiation polarization (Fig. 1.). Antennas are quasi double-bowtie type, with respectively a DC (direct coupling) antenna and a CC (capacitive coupling) antenna, which are directly excited by the incident wave with a polarization along their respective bowtie axis. The current in the CC antenna is capacitively coupled to a sub-antenna located on the membrane via a lower stack level antenna. The current flowing in the antennas is dissipated in load resistances that heat up the bolometer suspended membrane of the microbridge proportionally to the impinging optical (THz) power.

#177935 - $15.00 USD Received 11 Oct 2012; revised 19 Nov 2012; accepted 3 Dec 2012; published 20 Feb 2013

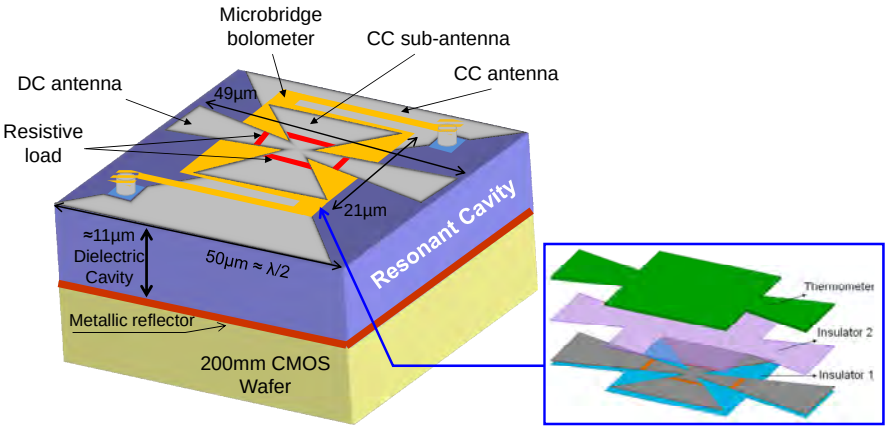


Fig. 1. Sketch of a single pixel of the microbolometer array with a detailed view of the sensitive stacked membrane shown in the inset.

The antennas are cavity-backed to improve the optical absorption efficiency of the structure. The quarter wavelength cavity is made of a 11-µm thick oxide layer deposited above a metallic reflector. Electrical connection between the bolometer sensor level downwards the CMOS read-out circuit upper metal pads is provided by copper-plugged through-silicon vias.

This sensor design provides a high frequency agility since the THz electromagnetic resonance of the pixel can be easily tuned through adjustment of the antenna geometry, pixel pitch and cavity height while preserving the bolometer central structure unchanged. Hence, for any targeted frequency range, sensitivity and time response remain optimum.

### *2.2 Integration into a 320 x 240 array*

The process of THz antenna-coupled microbolometer arrays is fully compatible with standard silicon microelectronic equipment. Arrays of 320 × 240 bolometers have been collectively processed above CMOS wafers integrating a CEA-Leti designed application specific integrated circuit (ASIC). The pixel pitch is 50 µm and the capacitive coupling antenna design is optimized for maximum sensitivity around 2.5 THz, which corresponds to the central frequency of a QCL that we used in a previous experiment [18].

The ASIC, derived from thermal infrared bolometer read-out designs, performs the measurement of bolometer resistances and formats the result in a single video data stream. This read-out-integrated circuit continuously scans the array in a row wise reading scheme where THz bolometers are voltage biased and the resulting current is amplified through capacitance trans-impedance amplifiers. Pixel voltage signal is multiplexed towards a video output which is digitalized and processed by a dedicated FPGA-based imager.

The prototyped device combined to its electronics results in a real-time THz camera with a large optical sensing area of 16 × 12 $mm^2$.

### *2.3 Detector spectral response*

The spectral sensitivity of the microbolometer has been determined by simulating the absorption coefficient of the device versus the wavelength of the incoming THz beam using a 3D electromagnetic solver (HFSS®) coupled to a multiphysics approach for the thermal behaviour (Comsol®). Using a Fourier Transform spectrometer (Bruker Vertex V80), the modelling has been validated from 3 THz down to 900 GHz by comparison with the experimental spectral dependence of the electrical signal delivered by a single pixel bolometer [19]. Absolute measurement of the CMOS-THz bolometer array response has been performed at 2.5 THz with a QCL source calibrated by a Thomas Keating powermeter: the bolometer responsivity at 2.5 THz is 16 MV/W [18]. The spectrum of the deduced absorption of the device is given in Fig. 2. As designed, the response peaks around 2.2 THz with an absorption

#177935 - $15.00 USD Received 11 Oct 2012; revised 19 Nov 2012; accepted 3 Dec 2012; published 20 Feb 2013

close to 90%, but presents a broadband behaviour with a full width half maximum (FWHM) larger than 2 THz. Optimal absorption of the device is mainly limited by the matching efficiency of loads and antennas. Bolometer threshold detection of the array is of the order of 30pW at 2.5THz [18]. At other frequencies, responsivity and consequently threshold detection will be mitigated by the spectral absorption of the device (Fig. 2.).

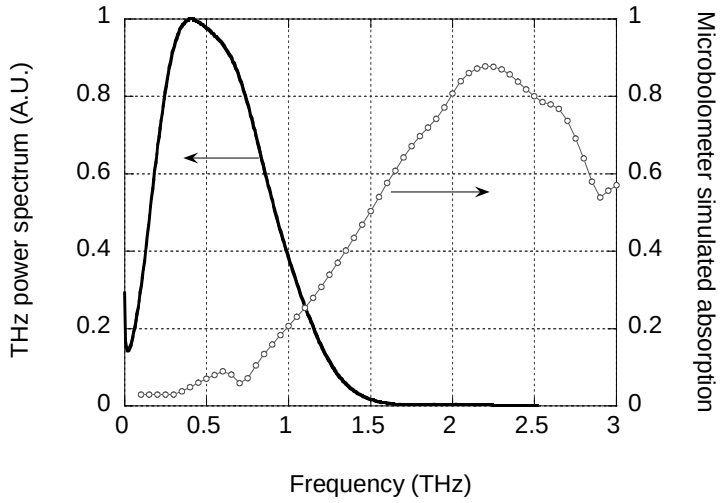


Fig. 2. Simulated absolute microbolometer spectral absorption for THz electrical field polarization aligned to the CC antenna (open circles, right vertical scale). Typical THz power spectrum delivered by the optoelectronics set-up and measured by a photoconductive antenna (continuous line, left scale).

*2.4 Signal acquisition and basic image processing*

The array ROIC is operated at 25Hz. In order to compensate slow thermal fluctuations of the detector, the acquired images are systematically subtracted to a reference image that is recorded every few seconds while the THz signal is blocked by a mechanical shutter. Signal to noise ratio (SNR) could be improved by averaging consecutive frames but this not the case in presented measurements. The frame time acquisition is 40ms and is kept constant for all acquisitions independently of signal level.

The electrical signal delivered by each pixel is numerically digitized by a 14-bits CMOS ADC with a 3.3-V dynamics leading to a least significant bit (LSB) value of about 200 µV. After data acquisition, the raw images are basically processed thanks to home-made routine software. This procedure consists in setting to the null value each noisy cell consisting in one or two pixels whose level is lower than 3 LSB. We shall note that this procedure is only used to reduce the background noise level of images. It does not affect the recorded THz images as it is not applied to pixels whose neighbors deliver a signal larger than 3 LSB. Moreover, considering wavelengths in the 0.1 to 3 mm range (0.1 to 3 THz), the size of one pixel (50 µm) is smaller than the diffraction limit, so tiny isolated details of the images are not altered by this procedure. In addition, one has to point out that, since both the source and the sensor are broadband, the image details are resulting from multispectral features.

## 3. Broadband optoelectronic set-up

The broadband THz signal used in this experiment is the output of a set-up based on a femtosecond laser (Femtosecond Laser Synergy) delivering an average power of 0.8 W at the repetition rate of 75 MHz. Ultrashort (FWHM 15 fs at the laser output) and broadband (85 nm centered around 800 nm) laser pulses are used to generate THz transients in a photoconductive emitter. This antenna (Laser-Quantum TeraSed) [20,21] consists of inter-digitated electrodes, separated by 5 µm, that are biased under a 15-V DC voltage,

#177935 - $15.00 USD Received 11 Oct 2012; revised 19 Nov 2012; accepted 3 Dec 2012; published 20 Feb 2013

corresponding to an estimated biasing electrical filed of 30 kV/cm. The laser average power at the emitter location can be adjusted from 30 to 300 mW using optical neutral density filters. The laser spot size at the photoconductive antenna is adjusted with a $f$ = 300 mm focusing lens to maximize the emitted THz power around 1 THz [21,22]. Using a pair of wire grid polarizers, we have verified that the THz beam is linearly polarized. As shown in the sketch of the experimental bench (Fig. 3), the broadband THz polarized signal is collected by a metallic off-axis parabolic mirror ($f$ = 50 mm), reflected by a flat copper mirror and then focused onto the detector by means of a second parabolic mirror similar to the first one or by a Teflon lens ($f$ = 50 mm).

In order to get more information about the spectrum of the emitted signal, we replaced the bolometer array by a photoconductive antenna (Ekspla-Teravil) activated by a weak delayed part of the laser beam as shown in Fig. 3. This modified scheme constitutes in fact a THz-TDS set up. The receiving antenna is made of a LTG-GaAs photoswitch together with a hyper hemispherical high-resistivity silicon lens that is optimized for collecting incoming parallel THz beams, whereas our recorded THz beam is actually focused. The modulus of the Fourier transform of the THz waveform recorded with this set up is shown in Fig. 2. The waveform data has been time-windowed to artificially remove the signal ripples due to water vapor absorption or to the rebounds of the THz beam in the emitter or in the high-resistivity silicon lens. The recorded TDS spectrum peaks around 400 GHz with a 750-GHz FWHM. Let us notice that it corresponds to the convolution of the THz signal focused at the receiver location by the spectral response of the detection apparatus. Thus, it is not the actual spectrum of the radiation that illuminates the microbolometer array and it is probably bandwidth limited. Nevertheless, both TDS spectrum and microbolometer array responsivity overlap and we estimate that at least one tenth of the overall incoming signal will be absorbed by the microbolometers.

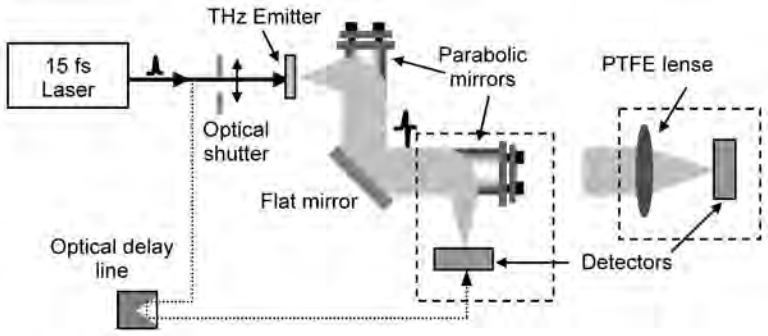


Fig. 3. Experimental set-up: The rectangular dashed areas show the two different focusing schemes. The detector can be of different type: microbolometer array, pyroelectric powermeter or photoconductive antenna. The dotted line corresponds to the additional optical path used to trigger the photoconductive detector when the experiment is set in the THz- TDS configuration (see paragraph 3 for more details).

## 4. Results and discussion

### *4.1 THz Beam imaging*

First images of broadband THz beams are obtained by placing the array of microbolometers at the focal point of the second parabolic mirror as shown in Fig. 3. The orientation of the array is adjusted so that the THz electrical field will be detected by the CC antenna. For the largest available THz power and the set-up finely adjusted, we record images similar to the one plotted in Fig. 4 (see also Fig. 5(a) and 5(b) for a 1D view of the same THz beam). This picture shows that the focused beam consists approximately in a fundamental Gaussian beam perturbed by two lower side lobes. As described in Fig. 5, the FWHM of the focused beam is in between 6 and 7 pixels, corresponding to widths of 320 µm in the horizontal plane and 340

#177935 - $15.00 USD Received 11 Oct 2012; revised 19 Nov 2012; accepted 3 Dec 2012; published 20 Feb 2013

µm along the vertical one. The peak voltage given by the pixel delivering the highest signal is $V_{max} = 332.5$ mV while the standard deviation of background level noise is 0.43 mV giving a SNR of 29 dB. Moreover, the noise level is independent of the THz signal amplitude.

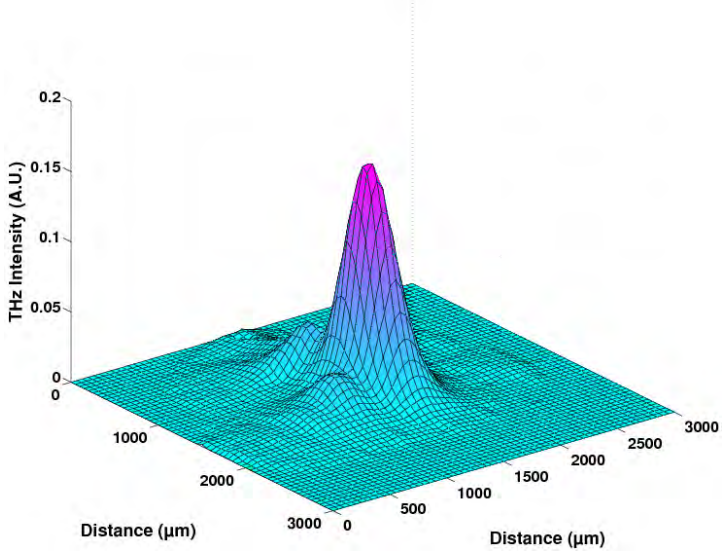


Fig. 4. Image of the broadband THz beam as focused by a parabolic mirror

To estimate the total absorbed THz power, we calculate the signal integrated over a circular surface centered on the location of the maximum of the beam shape and whose radius is 60 pixels, i.e. much larger than the beam average radius. In the case of Fig. 4, this integrated value is $V_{integrated} = 32.18V$. From this value, we then define an effective area $S_{eff}$ as $S_{eff} = V_{integrated} / V_{max}$. It corresponds to the number of pixels delivering the maximal signal $V_{max}$ that would be needed to get all the THz power integrated over a beam of arbitrary shape [23]. In the case of Fig. 4, the value of $S_{eff}$ is approximately 97 pixels.

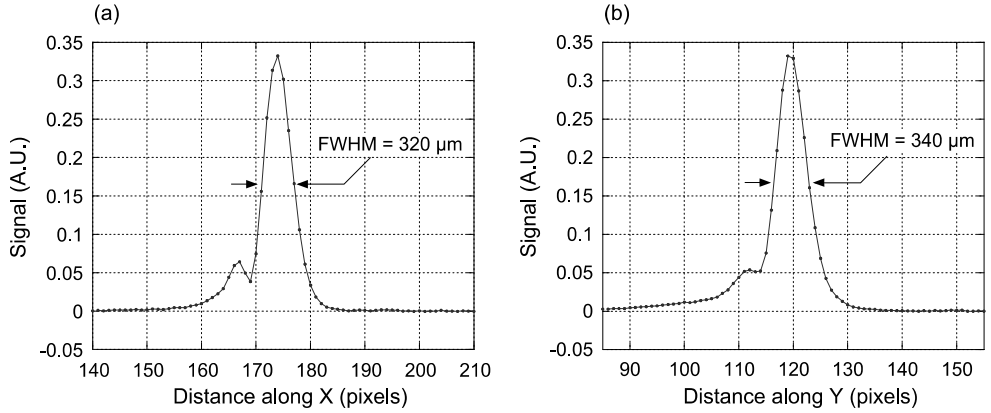


Fig. 5. (a) Horizontal THz beam profile. (b) Vertical THz beam profile.

### *4.2 Imaging of low power beams*

From the electrical signal delivered by the microbolometer array and the detector responsivity (16 MV/W), the noise level in all our experiments is estimated to be 27 pW. The detected integrated THz power is estimated to be 2.3 µW when the photoconductive emitter is driven by a laser average power of 320 mW and biased by a 15-V DC voltage (Fig. 4). As discussed

#177935 - $15.00 USD Received 11 Oct 2012; revised 19 Nov 2012; accepted 3 Dec 2012; published 20 Feb 2013

before, considering that most of the power is emitted around the 1-THz region where the responsivity of our detector is not optimized, this detected amount of power should correspond to a received THz power ranging approximately from 10 to 20 µW. This value is roughly confirmed by measuring the THz power with a pyroelectric detector (Gentec THz9B-MT) that gives a value of 5 µW after correction from the absorbance of this device which is reduced for frequencies lower than 1 THz. Moreover, considering the experimental parameters (IR average power and electrical biasing field) that we used to generate THz bursts into the large area photoconductive emitter, our estimation of the generated THz power is in good accordance with the one published by Dreyhaupt *et al.*, who characterized such an emitter using similar optical arrangement [21]. Concerning the THz power dependence upon optical power exciting the photoconductive antenna, these authors observed that, in such a large scale antenna, the THz emitted power varies quadratically with the optical power. Based on this observation, we checked the linearity of the microbolometer by varying the pump optical power. The peak amplitude of the detected signal and the integrated signal (not shown here) increase quadratically with the laser power (Fig. 6(a)), demonstrating the linearity of the bolometers response.

From this experiment, we estimate that the lowest IR excitation power of 34 mW corresponds approximately to a detected integrated THz power of 25 nW. Even for such a low power, the image quality (see the inset of Fig. 6(b)) is still good and allows one for the observation of the faintest details such as the lateral lobes already seen in Fig. 4 for higher power. Actually, for this low power image, the SNR of 10 (the peak voltage of 4.2 mV is 10 time larger than the standard deviation of the background noise level, i.e. 0.41 mV) permits some qualitative measurements such as the beam FWHM (Fig. 6(b)). This later is equal to 6 pixels in the horizontal direction and 6.5 pixels along the vertical one, as for the picture obtained with higher powers (Fig. 5), therefore the effective surface area $S_{eff}$ of the beam (96.8 pixels) is similar to the one measured at higher powers. We then estimate that the average power exciting a pixel is 0.26 nW in this measurement.

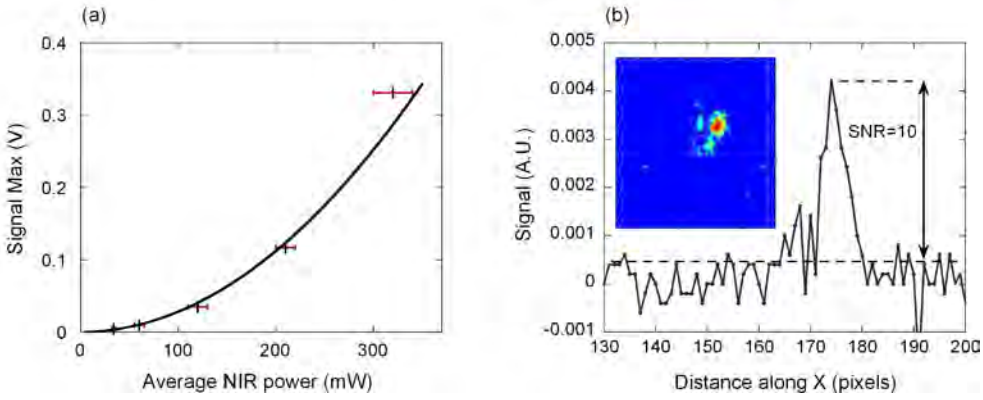


Fig. 6. (a) Optical power dependence of the detected peak THz signal. The crosses indicate the experimental data and the error bars obtained from the power measurement P. Full line shows the best fit proportional to $P^2$. (b) Horizontal beam profile for an estimated detected THz power of 25 nW. The dashed lines show the noise level and the maximal signal level. Inset: the corresponding 2D image with axis ranges corresponding to a surface of 70 x 75 pixels.

### *4.3 Focusing broadband signals*

The quality of the focused beam is very sensitive to both the performance of the optics and the accuracy of the set-up alignment. These features are particularly critical when working with broadband signals such as the one we are dealing with or with optoelectronic systems offering much larger THz range [24]. Actually, the wavelength of our system is covering more than one decade, ranging from 2 mm (0.15 THz) down to 0.2 µm (1.5 THz), making the spot size very sensitive to any chromatic aberration induced by the use of dispersive material. In order

#177935 - $15.00 USD Received 11 Oct 2012; revised 19 Nov 2012; accepted 3 Dec 2012; published 20 Feb 2013

to get rid of this problem, we use parabolic metallic mirrors that also reduce the optical losses in our set up. On the other side, such optics that is commonly used in optoelectronic THz-TDS setups and spectrometers is very sensitive to geometrical aberrations which induce distortion of the Gaussian feature of focused beams [25].

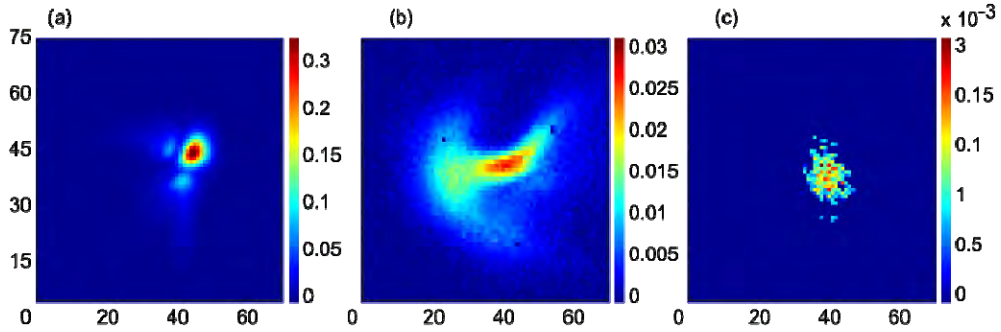


Fig. 7. 2D images of a focused beam using a $f$ = 50 mm optics consisting in: (a) a parabolic mirror that is correctly adjusted, (b) a misaligned parabolic mirror, (c) a PTFE doublet. All images correspond to the same surface of 70 x 75 pixels.

This is clearly observed in Fig. 7 where we compare the picture obtained for well-adjusted mirrors (Fig. 7(a)) to the one recorded for a slightly misaligned focusing mirror (Fig. 7(b)): the coma aberration is clearly seen in this latter case [26]. Finally, in Fig. 7(c), we show the beam as focused by a $f$ = 50 mm biconvex doublet made of two plano-convex Teflon (PTFE) lenses stacked together. In this case, the adjustment of the lens is rather easy and one can observed that the spot does not suffer from any geometrical aberration and its effective area $S_{eff}$ is similar to the one recorded in Fig. 7(a). Unfortunately, in this case, the broadband signal suffers from strong absorption by the 2.76-cm thick focusing optics and only 1.5% of the total power detected in Fig. 7(b) is recorded now. This is explained by the absorption coefficient of Teflon which is ranging from 0.1 to 3 $cm^{-1}$ in the 0.5-2 THz region [27].

## 5. Conclusion

In conclusion, we used a 320 x 240 array of antenna-coupled microbolometers with integrated CMOS read-out electronics to characterize THz beams generated by a photoconductive antenna driven by a femtosecond laser oscillator. Our measurements were performed at room temperature and real time images were routinely obtained for average detected power in the µW-nW range. Thanks to a low noise level of 27 pW, we have usefully characterized a THz beam with detected power as low as 25 nW corresponding to a power per pixel of 0.28 nW, that is equivalent to a SNR of 10. This demonstrates the ability of such detector to be used with most common THz time-domain spectroscopy set-ups that are regularly employed for broadband THz material and device characterization. Moreover, the 50-µm pitch of our array allows getting precise information about the geometrical features of the THz beam imaged by a large sensitive area (12 x 16$mm^2$). Further works will target improved absorption of the detector in lower frequency range below 1 THz. These improvements will be achieved by modification of antenna design while preserving pixel pitch, ROIC and current technological stack [28]. Such developments are motivated by benefits of this camera that proved to be of decisive help to align any THz set-up in real time.

## Acknowledgments

This work was supported in part by the ANR-JST France-Japan International Strategic Collaborative Research Program ‘‘Wireless communication using Terahertz plasmonicnano ICT devices’’ (WITH).

#177935 - $15.00 USD Received 11 Oct 2012; revised 19 Nov 2012; accepted 3 Dec 2012; published 20 Feb 2013